Cu-Mn oxygen carrier with improved mechanical resistance: Analyzing performance under CLC and CLOU environments

Fuel Processing Technology 217 (2021) 106819

Contents lists available at ScienceDirect

Fuel Processing Technology

journal homepage: www.elsevier.com/locate/fuproc

Cu-Mn oxygen carrier with improved mechanical resistance: Analyzing performance under CLC and CLOU environments

Iñaki Adánez-Rubio [a,*], Amanda Nilsson [b], María Teresa Izquierdo [a], Teresa Mendiara [a], Alberto Abad [a], Juan Adánez [a]

[a] Instituto de Carboquímica (ICB-CSIC), Dept. of Energy & Environment, Miguel Luesma Castán, 4, Zaragoza 50018, Spain
[b] Department of Chemical and Biological Engineering, Division of Environmental Inorganic Chemistry, Chalmers University of Technology, SE-412 96 Göteborg, Sweden

ARTICLE INFO

Keywords:
CO_2 capture
CLOU
Copper
Solid fuels
Manganese
Kaolin

ABSTRACT

Chemical Looping Combustion process allows combustion of gaseous, liquid or solid fuels with CO_2 capture. The oxygen necessary for combustion can be supplied using lattice oxygen (CLC) or oxygen uncoupling (CLOU) mechanisms. The present work studies the effects of kaolin addition on Cu—Mn oxygen carrier behavior for CLC and CLOU processes. Cu—Mn oxygen carrier was prepared by granulation with a composition: 27.2 wt% CuO, 52.8 wt% Mn_3O_4 and 20 wt% kaolin. Oxygen release rates and fluidization behavior were analyzed by TGA and batch fluidized bed reactor. The oxygen carrier was studied for CH_4 and synthetic biogas combustion in a 500 W_{th} CLC continuous unit for 50 h of combustion at temperatures up to 930 °C. No agglomeration problems were observed. Results found during biogas combustion were similar to methane combustion. The addition of 20 wt% kaolin changed the mixed oxide chemical composition generating $Cu_{1.2}Mn_{1.8}O_4$ and improved significantly the oxygen carrier mechanical resistance, increasing the extrapolated lifetime to 19,000 h, 3.6 times over the value found for any Cu based oxygen carrier in CLC. However, the oxygen carrier reactivity had an important decrease with respect to a similar oxygen carrier without kaolin addition, whose fraction in oxygen carrier must be optimized.

1. Introduction

The growing increase of CO_2 concentration in the atmosphere as a consequence of the anthropogenic CO_2 emissions coming for fossil fuel use in energy production is favoring the increase of the natural greenhouse effect. One important part of the 33.1 $GtCO_2$ released in 2018 came from energy generation sector [1]. In fact, fossil fuels represent around 80% of the world primary energy demand. There is a general agreement on the need to reduce CO_2 emissions to the atmosphere that was reflected in the Paris Agreement, which aims to limit the global temperature increase to less than 2 °C by 2100 [2]. Different actions such as improvement in energy efficiency, deployment of renewable energy and implementation of Carbon Capture and Storage (CCS) technologies should be taken to reach that objective. Moreover, Bio Energy with Carbon Capture and Storage (BECCS), which combined the use of biofuels together CCS, would contribute to reach negative CO_2 emissions that are needed to meet the Paris Agreement objective.

From both technical and economic point of view, Chemical Looping Combustion (CLC) is considered as one of the most efficient ways for the CO_2 capture needed in CCS technologies. The process is commonly carried out in two interconnected reactors (Fig. 1). Combustion oxygen is transferred to the fuel by means of a metal oxide (Me_xO_y) without contact with the air. Fuel is oxidized to CO_2 and H_2O while the metal oxide is reduced in the fuel reactor (r1). The reduced metal oxide (Me_xO_{y-1}) is regenerated with air in the air reactor (r2). The global enthalpy is the same as the conventional combustion with no inherent energy penalty for the process (r3). After steam condensation a highly concentrated CO_2 stream is ready for storage. This technology is highly promising for power plants due to its inherent CO_2 capture with very low global energy penalty.

$$(2n+m-p)M_xO_y + C_nH_{2m}O_p \rightarrow (2n+m-p)M_xO_{y-1} + nCO_2 + mH_2O \quad \Delta H_r \qquad (r1)$$

$$(2n+m-p)M_xO_{y-1} + \left(n+m/2-p/2\right)O_2 \rightarrow (2n+m-p)M_xO_y \quad \Delta H_o \qquad (r2)$$

* Corresponding author.
E-mail address: iadanez@icb.csic.es (I. Adánez-Rubio).

https://doi.org/10.1016/j.fuproc.2021.106819
Received 24 November 2020; Received in revised form 15 February 2021; Accepted 11 March 2021
Available online 23 March 2021

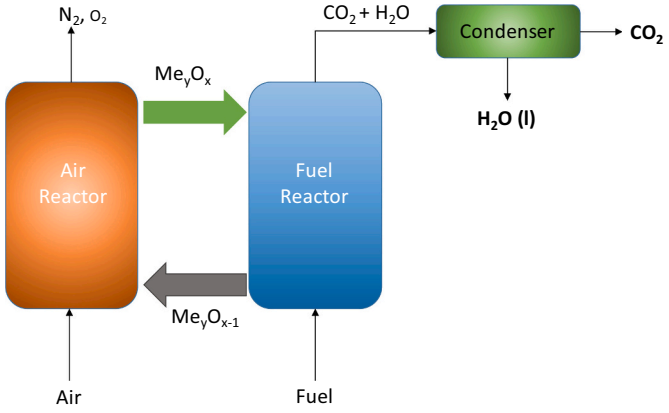

Fig. 1. Chemical looping combustion diagram.

$$(2n+m-p)M_xO_y+\left(n+m/2-p/2\right)O_2 \rightarrow nCO_2+mH_2O\ \Delta H_c=\Delta H_r+\Delta H_o \quad \text{(r3)}$$

CLC was initially developed for gaseous fuels and afterwards adapted for solid fuels. An overview of the CLC process can be found in some review papers from Hossain et al. [3], Lyngfelt et al. [4,5], Fan [6], Zhao et al. [7] and Adánez et al. [8]. A specific review for solid fuels CLC can be found in Adánez et al. [9]. The performance of the oxygen carrier material is the cornerstone of the Chemical Looping technology. Different types of oxygen carriers have been proposed in the literature as synthetic materials, prepared using the active metal oxides (NiO, CuO, Fe_2O_3, Mn_2O_3) supported on different inert materials, mixed oxides containing in their structures Fe, Cu, Mn and Ca oxides, and ores of iron and manganese or metal oxide wastes (red mud, LD slag). Some authors also developed models for CLC of solids fuels [10,11].

Copper based oxygen carriers have demonstrated to have suitable properties for Chemical Looping Combustion of gaseous and solid fuels [8] both supplying lattice oxygen (CLC) [12] or gaseous oxygen [13,14] by Chemical Looping with Oxygen Uncoupling (CLOU). The supply of lattice oxygen is the most common reaction mechanism present in Chemical Looping processes. However, some CuO and Mn_3O_4 based oxygen carriers can release gaseous oxygen at high temperatures depending on its composition and operating conditions. CuO based oxygen carriers and some mixed oxides [15] allow complete combustion to CO_2 and H_2O by both mechanisms burning gaseous [8] or solid fuels [16,17]. Attention has to be paid to CuO carriers in gaseous fuels combustion in order to avoid agglomeration problems that appear with high CuO fractions and high reaction temperatures originated by the low melting point of Cu (1083 °C). De Diego et al. [18] found that impregnated CuO/Al_2O_3 oxygen carriers with a CuO content greater than 20 wt % always agglomerated during CH_4 combustion in batch fluidized bed cycles. For CuO contents from 15 to 17 wt% CuO the agglomeration behavior depended on the calcination temperature, while for lower CuO fractions agglomeration was not observed. Cu-based oxygen carriers prepared by dry impregnation using γ-Al_2O_3 as support were evaluated during the combustion of CH_4, in CLC pilot units, reaching a good performance in terms of combustion efficiency [12,19–21] at low oxygen carrier to fuel ratios operating at 800 °C. Moreover, the lifetime estimated from attrition data during combustion in a continuous unit depended on the support properties. Lifetimes of 2500 h [19] and 5000 h [22] were found for two different γ-Al_2O_3 supports.

Moreover, CuO based oxygen carriers were developed and used to demonstrate the proof of the concept for CLOU combustion for coal and biomass [16,23–25] showing excellent performance regarding CO_2 capture and reaching always a complete combustion of fuel reactor gases, avoiding the need of use of one oxygen polishing step [9], usually needed if the mechanism for oxygen transfer is based on lattice oxygen. However, these oxygen carriers need lifetime improvement and CuO content reduction in order to reduce carrier costs.

Cu—Mn mixed oxides were investigated with the objective to reduce the drawbacks of the individual parent oxides. Driessens et al. [26] investigated the system Cu-Mn-O at different metal molar ratios and temperatures finding mixed oxides with different crystalline structures and variable compositions. Azad et al. [27] investigated mixed oxides $Cu_xMn_{3-x}O_4$, prepared with a ratio Cu:Mn 1:1 calcined at two temperatures and analyzed their capability for burning CH_4 and for releasing gaseous oxygen by CLOU. At the same time, a detailed analysis of fresh, reduced and oxidized active phases was developed. Hosseini et al. [28] carried out the characterization and determined the oxygen release capability of Cu—Mn mixed oxides with different Cu/Mn ratios, finding the excellent CLOU capability under relevant conditions in a fluidized bed at 800 °C burning coal char. Adánez-Rubio et al. [29] investigated the mixed oxide $Cu_{1.5}Mn_{1.5}O_4$ prepared by calcination of hopcalite at 950 °C for CLOU process. CLOU behavior was investigated by TGA and in batch fluidized bed burning char and its parent coal. High oxygen release rates with char were found reaching a maximum value of $0.62.10^{-3}$ kg O_2/ s. kg oxygen carrier, showing the capability of this mixed oxide for solid fuel combustion by this process. Adánez-Rubio et al. developed and tested the combustion of coal [30–32] and biomass [24,25,33] with one mixed oxide $Cu_{1.5}Mn_{1.5}O_4$ prepared by fluidized bed granulation with a 34% CuO and 66% Mn_3O_4 and calcined two hours at 1125 °C. $Cu_{1.5}Mn_{1.5}O_4$ showed high reactivity and oxygen carrying capacity. For CLC using lattice oxygen, the Cu—Mn mixed oxide was reduced to Cu and MnO as well as during oxidation at operating conditions the mixed oxide structure $Cu_{1.5}Mn_{1.5}O_4$ was recovered. This mixed oxide was reduced and oxidized according to reactions [r4] and [r5].

$$8Cu_{1.5}Mn_{1.5}O_4+5CH_4 \rightarrow 12Cu+12MnO+5CO_2+10H_2O \quad \text{(r4)}$$

$$6Cu+6MnO+5O_2 \rightarrow 4Cu_{1.5}Mn_{1.5}O_4 \quad \text{(r5)}$$

Depending on the operating temperature and O_2 concentration in the gas, $Cu_{1.5}Mn_{1.5}O_4$ can be decomposed releasing gaseous oxygen allowing CLOU process with direct reaction between fuel and gaseous oxygen [31] (r6).

$$2Cu_{1.5}Mn_{1.5}O_4 \leftrightarrow 3CuMnO_2+O_2 \quad \text{(r6)}$$

Excellent results were found reaching complete combustion of fuel reactor gases and high CO_2 capture efficiencies with this oxygen carrier burning different solids fuels at CLOU conditions. After 50 h of combustion of coal and biomass the oxygen carrier showed an increase in the fines generation indicating that the material started to be destroyed. Attrition behavior was also followed considering the Attrition Jet Index (AJI) of the fresh oxygen carrier calculated as 3.0. After 30 h of continuous operation burning coal at ϕ values lower than 3, AJI value suffered a moderate increased reaching a value of 16.0 [28] indicating that particle integrity started to be reduced.

Thus, a considerable number of oxygen carriers with high reactivity in CLC and CLOU, some of them based on Cu—Mn mixed oxides with excellent combustion results, have been developed. However, the number of oxygen carrier materials with stable mechanical performance after long-term operation in a CLC unit is very limited. This is a limitation for the scale-up of the CLC process. It is imperative to find materials that maintain their mechanical properties during CLC operation. In order to enhance the mechanical integrity of a material based on Cu—Mn mixed oxide, the use of one ceramic binder as kaolin has been examined in this work to know the oxygen carrier performance for CLC/CLOU processes.

The aim of this investigation was to develop Cu—Mn mixed oxide oxygen carriers with CLOU/CLC properties with enhanced mechanical resistance to improve its lifetime. Capability of gaseous oxygen release and lattice oxygen supply was evaluated together the mechanical resistance in order to consider its use for CLOU/CLC combustion in a continuous unit of two interconnected fluidized beds burning CH_4 and

Table 1
Properties of the oxygen carrier particles.

	Fresh	Used 50 h
Oxygen transport capacity, R_{OC} (wt%)	12.5	13.1
Oxygen transport capacity CLOU, R_{CLOU}	4.1 2.4	4.1 2.1
Crushing strength (N)		
Skeletal density of particles (kg/m^3)	4241	4366
AJI (%)	0.9	11.2
Porosity (%)	8.5	44.3
Specific surface area, BET (m^2/g)	0.1	1.4
Main species	$Cu_{1.2}Mn_{1.8}O_4$, Mn_3O_4, Mn_2O_3	$Cu_{1.2}Mn_{1.8}O_4$, $CuMnO_2$, Cu_2O, Cu, MnO, Mn_2SiO_4

synthetic biogas.

2. Experimental section

2.1. Materials

A mixed oxide of Cu and Mn with similar composition to the previously developed [31] was prepared with the addition of a ceramic binder as kaolin in order to improve its mechanical resistance. Particles were prepared by fluidized bed granulation in a spouted fluidized bed system, Procell LabSystem Glatt. As raw materials CuO (Chem-Lab), Mn_3O_4 (Micromax ELMAX) and kaolin (SICA S.L) were used. A solid suspension containing about 80% of solids and different additives was prepared for granulation. A physical mixture of powders was prepared containing 27.2 wt% CuO, 52.8 wt% Mn_3O_4 and 20% kaolin. After granulation particles were calcined at 1025 °C for 2 h. The oxygen carrier prepared was named as CuMn80-Kao20 based in the weight percent distribution. Particles were sieved to a particle size +100–300 μm for fluidization.

2.2. Oxygen carrier characterization

Chemical and physical characteristics of the oxygen carrier were determined by different methods. Crushing strength, jet attrition test index, particle size, pore volume, density, specific surface area and crystalline phases were analyzed. Oxygen transport capacity for CLC (R_{OC}) was determined through the weight loss obtained in TGA by reduction with H_2 at 800 °C, while the oxygen transport capacity for CLOU (R_{CLOU}) was measured in N_2 atmosphere at 900 °C. Table 1 shows the main physical and chemical characteristics of the oxygen carrier particles.

The crushing strength of the carrier particles was determined in a Shimpo FGN-5× crushing strength apparatus as an average value of 20 measurements, with particles sized +0.1–0.3 mm. A three-hole air jet attrition equipment ATTRI-AS (Ma. Tec. Materials Technologies Snc) configured according to the ASTM-D-5757 standard [34] was used to determine the low temperature attrition resistance. The Attrition Jet Index value (AJI) was calculated considering the weight of fine particles recovered in the filter after 5 h of testing by this equation.

$$\mathrm{AJI} = \frac{m_{5h}}{m_s} \quad (1)$$

where m_{5h} is the mass collected of fines after 5 h from the attrition tester, and m_s is the mass of sample loaded into the system (nominally 50 g).

He picnometry was used to determine the skeletal density of the oxygen carrier particles by a Micromeritics AccuPyc II 1340. BET specific surface area was determined by Brunauer-Emmett-Teller (BET) method based on nitrogen adsorption/desorption at 77 K in a Micromeritics ASAP-2020 instrument (Micromeritics Instruments Inc.). Pore volume was measured by Hg intrusion using a Quantachrome PoreMaster 33 porosimeter. Crystalline chemical species were identified by X-ray diffraction (XRD), with XRD patterns collected by a Bruker D8 Advance X-ray powder diffractometer equipped with an X-ray source with a Cu anode working at 40 kV and 40 mA, and an energy-dispersive one-dimensional detector. The diffraction pattern was obtained over the 2θ range of 10° to 80° with a step of 0.019°. The oxygen carrier particles were also analyzed by scanning electron microscopy (SEM) using an SEM-EDX Hitachi S-3400 N with analyzer EDX Röntec XFlash de Si(Li).

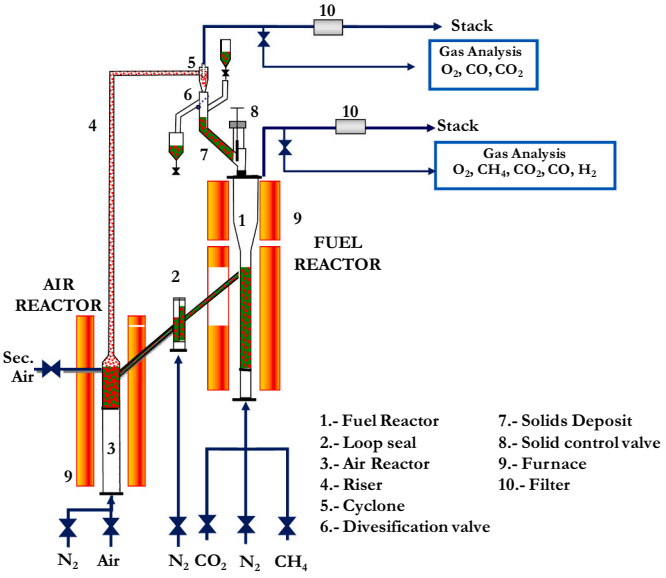

Fig. 2. Diagram of the 500-W_{th} continuous CLC system.

2.3. Experimental installations

2.3.1. TGA

To know the oxygen transport capacity of the oxygen carrier both for CLC and CLOU and its reactivity, multiple redox cycles were carried out in a TGA, CI Electronics type, previously described [35]. TGA reactivity of the oxygen carrier was measured for CLC through the weight changes with time with 15% CH_4 and 20% H_2O and oxidation in air, in the third cycle for fresh particles and used particles. The R_{OC} value was calculated in the third reduction cycle with 15% H_2 and 20% H_2O and oxidation in air. CLOU reactivity was measured in N_2 atmosphere during third reduction redox cycle in N_2/air at temperatures from 800 to 900 °C using 50 mg samples. First cycle reactivity measurement was made to know the reactivity of used particles and to allow the comparison with values found for fresh material. All the TGA experiments were carried out under conditions to ensure chemical reaction control as described in [35].

2.3.2. Batch fluidized bed reactor

The oxygen carrier behavior was investigated in a fluidized batch reactor with multiple redox cycles of oxygen release in N_2 and with methane combustion under similar conditions to that of CLOU/CLC processes. Moreover, the attrition during redox cycles and the agglomeration trends were determined. One batch fluidized bed reactor setup [36] with a 54 mm inner diameter reactor was used. A batch of 300 g of oxygen carrier particles was used as the bed material. The gas feeding system have different mass flow controllers for different gases and a peristaltic pump for water supply. Attrition rate calculation was made from the recovered elutriated solids from the bed in a heated filter during the successive reduction–oxidation cycles. Tests were carried out with an inlet superficial gas velocity of 0.15 m/s. Gas composition during reduction was 100 vol% N_2 or 25 vol% CH_4 with 20 vol% H_2O in N_2. During oxidation different oxygen concentrations were used ranging

Table 2
Experimental conditions and main result in the CLC unit. Bold number: condition varied for comparison purposes.

Test – fuel	$T_{FR}(^{\circ}C)$	$T_{AR}(^{\circ}C)$	$[O_2]_{AR}$ (%)	Φ	$\dot{m}_{OC}(kg/h)$	$C_{CH_4}(vol\%)$	Ratio CO_2/CH_4	*Power(W)*	$\dot{m}_{FR}(kg/MW)$	η_{Comb} (%)
C01 – CH4	750	800	21.00	28.4	16.80	7	0	224	1378	24.2
C02 – CH4	770	800	21.00	27.9	16.80	7	0	226	1368	27.7
C03 – CH4	800	800	21.00	27.9	16.80	7	0	217	1423	34.2
C04 – CH4	800	800	21.00	15.9	9.50	**7**	0	228	1372	31.7
C05 – CH4	800	800	21.00	15.6	13.30	**11**	0	318	971	34.5
C06 – CH4	**800**	800	21.00	14.4	17.20	**15**	0	460	671	36.9
C07 – CH4	**815**	800	**21.00**	11.7	13.95	15	0	462	668	43.0
C08 – CH4	815	800	**18.34**	11.7	13.95	15	0	461	669	40.5
C09 – CH4	815	800	**16.30**	11.7	13.95	15	0	458	674	40.8
C10 – CH4	815	800	**13.14**	11.7	13.95	15	0	455	678	40.9
C11 – CH4	**850**	810	21.00	12	14.35	15	0	468	659	55.0
C12 – CH4	**875**	810	21.00	12	14.35	15	0	461	669	55.3
C13 – CH4	**885**	810	21.00	12	14.35	15	0	458	674	57.1
C14 – CH4	**895**	810	21.00	12	14.35	15	0	456	677	60.5
C15 – CH4	**775**	810	21.00	9	13.10	15	0	516	1153	54.6
C16 – CH4	**800**	810	21.00	9	13.10	15	0	512	1162	60.4
C17 – CH4	**830**	810	21.00	9	13.10	15	0	516	1152	66.8
C18 – CH4	**850**	810	21.00	9	13.10	15	0	537	1108	74.5
C19 – CH4	**900**	810	21.00	9	13.10	15	0	543	1095	89.0
C20 – CH4	**925**	810	21.00	9	13.10	15	0	544	1093	91.9
C01 – Bio	800	810	21.00	9.3	14.70	20	**2**	622	955	65.7
C02 – Bio	**800**	810	21.00	9.3	14.70	20	**1.5**	622	955	62.9
C03 – Bio	800	810	21.00	9.3	14.70	20	**1**	622	955	63.7
C04 – Bio	800	810	21.00	9.3	14.70	20	**0.7**	622	955	64.8
C05 – Bio	800	810	21.00	9.3	14.70	20	**3**	622	955	64.5
C06 – Bio	**825**	**810**	**21.00**	**9.9**	15.95	20	1.5	642	927	71.3
C07 – Bio	**850**	810	21.00	9.9	15.95	20	1.5	642	927	77.7
C08 – Bio	**875**	810	21.00	9.9	15.95	20	1.5	642	927	82.9
C09 – Bio	**900**	810	21.00	9.9	15.95	20	1.5	642	927	87.4
C10 – Bio	850	**825**	21.00	9.6	15.00	20	1.5	653	911	87.0
C11 – Bio	850	**850**	21.00	9.6	15.00	20	1.5	653	911	87.7
C12 – Bio	**920**	810	21.00	9.6	15.00	20	1.5	653	911	90.4
C13 – Bio	850	810	**18.29**	9.6	15.00	20	1.5	653	911	75.5
C14 – Bio	850	810	**17.86**	9.6	15.00	20	1.5	653	911	76.1
C15 – Bio	850	810	21.00	**12**	19.00	20	1.5	642	926	75.3
C16 – Bio	850	810	21.00	**6**	9.00	20	1.5	642	926	74.5
C17 – Bio	850	810	21.00	**4.5**	7.00	20	1.5	642	926	75.4

where $\dot{m}_{FR}$ is the specific carrier inventory given in kg/MW.
Bold numbers for comparison purposes between experiments.

from 5 to 21 vol% O_2 in N_2.

The gas outlet from the fluidized bed reactor was connected to two parallel hot filters with one of them always connected and open towards the gas analyzer system. The outlet concentrations of CH_4, CO and CO_2 were measured by a Non-Dispersive Infra-Red (NDIR) analyzer (Maihak S710/UNOR) and the concentration of H_2 was measured by a Thermal Conductivity Detector (TCD), (MaihakS710/THERMOR). A paramagnetic gas analyzer (Siemens Oxymat 5E) measured the O_2 concentration evolution with time.

2.3.3. 500 W_{th} continuous unit

The performance of CuMn80-Kao20 in the combustion of CH_4 or synthetic biogas as fuel was studied in a 500 W_{th} CLC pilot plant at temperatures from 800 to 900 °C. Fig. 2 provides a schematic diagram of the continuous unit. The CLC unit consists of two bubbling fluidized bed reactors, the fuel reactor and the air reactor, connected by a loop seal; a riser for solids transport to a cyclone; a solids valve to control the solids circulation rate between both reactors; a diverting solids valve to take samples from the air reactor; a small deposit to take samples from the fuel reactor; and two filters to collect the elutriated fines during the process. Composition of the two outlet streams was analyzed with continuous analyzers. CO, CO_2, and CH_4 were analyzed by nondispersive infrared (NDIR) analyzers (Maihak S710/UNOR and Siemens Ultramat 23); O_2 by paramagnetic analyzer (Oxymat 6 and Siemens Ultramat 23); H_2 was measured using a thermal conductivity detector (Maihak S710/THERMOR). A more detailed description of the unit can be found in [37]. The total solids inventory in the continuous unit was 2.1 kg. Different CH_4 flows and two different bed heights of the fuel reactor were used to have different oxygen carrier inventories in the fuel reactor: from ca. 660 to 1400 kg/MW_{th}. Table 2 shows the main experimental conditions used in the tests.

The fuel reactor temperature was changed from 775 to 925 °C during the 50 h of continuous operation, i.e. 30 h burning CH_4 and 20 h burning synthetic biogas. Gas velocity in the fuel reactor was 0.15 $m{\cdot}s^{-1}$ using 300 $LN{\cdot}h^{-1}$. The loop seal was fluidized with N_2 (75 $LN{\cdot}h^{-1}$). The air reactor was fluidized by a primary air of (720 $LN{\cdot}h^{-1}$) introduced from the bottom of the bed, and a secondary air of 150 LN h^{-1} at the top of the air reactor to assist oxygen carrier entrainment in the riser. Different mixtures of CH_4, CO_2 and N_2 were used as fuel to analyze the behavior of CuMn80-Kao20 oxygen carrier in the combustion of natural gas and biogas. N_2 was used to dilute the fuel. Synthetic biogas with ratios CH_4/CO_2 from 0.7 to 3 were used.

2.4. Data evaluation

The conversion of the oxygen carrier was calculated as follows:
For reduction:

$$X_{Red} = \frac{m_{Ox} - m}{m_{Ox} - m_{Red}} \quad (2)$$

For oxidation:

$$X_{Ox} = 1 - \frac{m_{Ox} - m}{m_{Ox} - m_{Red}} \quad (3)$$

where m is the sample mass at each time, m_{Ox} is the fully oxidized sample mass and m_{Red} the sample weight in the reduced state.

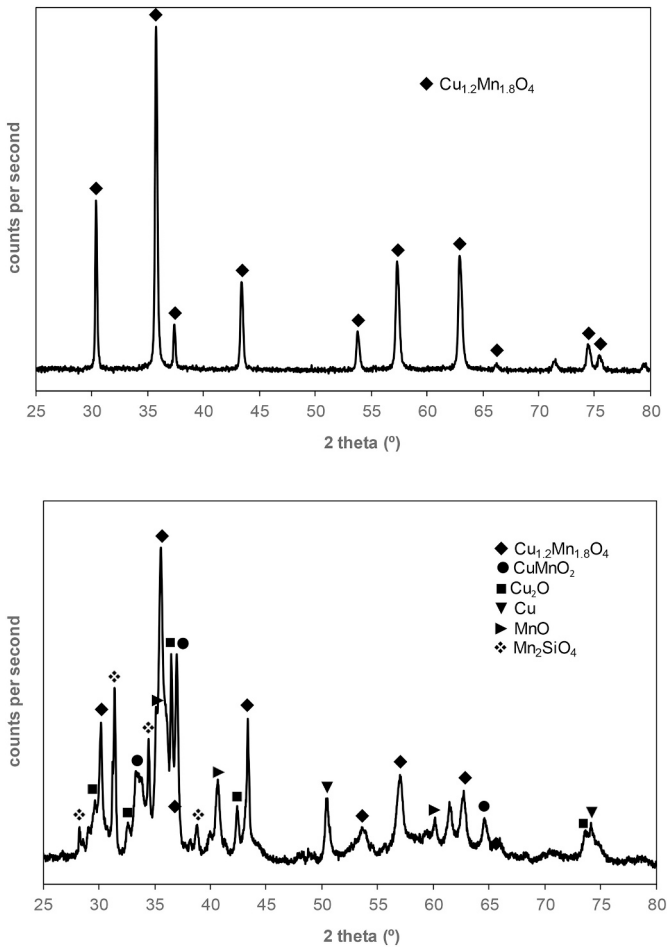

Fig. 3. XRD difractogram of fresh oxygen carrier sample (a) and reduced used oxygen carrier sample (b) main crystal phase marked.

The oxygen carrier-to-fuel ratio, ϕ, in the 500 W_{th} CLC unit is defined as the ratio between the flow of oxygen supplied by the oxygen carrier and the stoichiometric oxygen needed to fully burn the fuel, which is calculated as follows:

$$\phi = \frac{x_{Cu_{1.2}Mn_{1.8}O_4} F_{solids}}{F_{CH_4} M_{Cu_{1.2}Mn_{1.8}O_4}} \quad (4)$$

where $x_{Cu1.2Mn1.8O4}$ is mass fraction of $Cu_{1.2}Mn_{1.8}O_4$ in the oxygen carrier; F_{solids} is the mass-based oxygen carrier circulation rate inside the CLC unit and F_{CH_4} is the inlet molar flow of the CH_4 fed to the fuel reactor.

The combustion efficiency (η_{Comb}) was calculated (5) by knowing the fraction of oxygen needed for complete combustion of unconverted gases over the total oxygen for fuel conversion to CO_2 and H_2O.

$$\eta_{Comb} = 100 - \frac{(x_{CO} + x_{H_2} + 4 \cdot x_{CH_4})_{out} \cdot F_{out}}{(4 \cdot x_{CH_4})_{in} \cdot F_{in}} \quad (5)$$

where x_i is the molar fraction of i gas compound. F_{in} and F_{out} are the molar flows of the input and output gases.

The accuracy of the results was measured through the oxygen and carbon mass balances considering the measurements of gas analyzers from the fuel and air reactors in the overall unit; these balances closed always over 95%.

Table 2 shows the experimental conditions and main data results for the experimental campaigns performed in the 500 W_{th} continuous CLC unit burning CH_4 and synthetic biogas. In the 30 first hours of operation, the effect of fuel reactor temperature, the oxygen carrier to fuel ratio, CH_4 concentration in the fuel reactor and the air excess (related with the O_2 concentration fed to the air reactor, [$O_{2,AR}$]) in the air reactor on the combustion efficiency and the attrition rates were investigated using mixtures CH_4-N_2.

2.5. Attrition evaluation

The attrition resistance of the oxygen carrier was evaluated by two methods: (1) Air Jet Attrition index (AJI) determined in an ATTRI-AS equipment using ASTM-D-5757 standard; and (2) attrition rate measured in the continuous unit. Attrition rate was calculated as a function of the weight of particles collected in the filters of fuel and air reactors with size lower than 45 μm. The attrition rate, A (%/h), was calculated by

$$A = \frac{m_f}{m_t \Delta t} \cdot 100 \quad (6)$$

where m_f is the mass of the elutriated particles with a size lower than 45 μm recovered during Δt (hours), and m_t is the total mass of solids in the continuous CLC unit. With the attrition rate value obtained the extrapolated lifetime can be calculated by the following equation

$$LT\ (h) = \frac{100}{A} \quad (7)$$

3. Results

3.1. Results from oxygen carrier characterization

Physical and chemical properties of the oxygen carrier were determined for the fresh oxygen carrier. As expected both specific surface area (BET) and porosity showed low values and the crushing strength had a value of 2.4 N that is acceptable for its use in CLC fluidized beds [38]. Attrition Jet Index (AJI) that indicates the physical attrition resistance in fluidized bed reactor had a quite low value (0.9) indicating the initial suitability of the material for CLC, see Table 1.

XRD diffractograms of fresh and used oxygen carrier particles are shown in Fig. 3a and b, respectively. Analyzing the profiles with DIFFRAC.EVA software the phases that could be identified in fresh oxygen carrier were $Cu_{1.2}Mn_{1.8}O_4$, and some Mn_2O_3 and Mn_3O_4 remaining in the stabilized particles. No crystal phases containing Al or Si from the kaolinite were detected, indicating that they should be in the amorphous phase, and thus, it cannot be detected by XRD technique. The temperature of calcination of the oxygen carrier (1025 °C) exceeded temperature for dehydroxylation reaction of kaolinite at which amorphous background phase is only registered by XRD [39].

The content of different species in the crystalline phase of fresh sample was determined after calcination by Rietveld refinement and further the composition was corrected considering the 20% kaolin that was not detected by XRD after calcination. The composition of the oxygen carrier particles was the following: 75.1 wt% of $Cu_{1.2}Mn_{1.8}O_4$, 0.7 wt% of Mn_2O_3, 4.2 wt% of Mn_3O_4 and 20 wt% of kaolin. Although the same Cu:Mn ratio than the previous work was originally used in the preparation [31], the main mixed oxide generated was $Cu_{1.2}Mn_{1.8}O_4$ but not $Cu_{1.5}Mn_{1.5}O_4$. The only difference between both Cu—Mn samples was the calcination temperature (1150 °C originally and 1025 °C in this work) now. It is necessary to indicate that according with Driessens [26] diagram, differences in chemical and crystalline structures should not be found. XRD patterns of reduced sample extracted from fuel reactor (Fig. 3b). It can be seen that the main phases are $Cu_{1.2}Mn_{1.8}O_4$, $CuMnO_2$, Cu_2O, Cu, MnO and Mn_2SiO_4. In order to understand the phases that can be appeared in function of CLC or CLOU reactions, several experiments were carried out in the TGA with N_2 and CH_4. After reduction in N_2 the reduced compounds found were $CuMnO_2$, Mn_3O_4 and Cu_2O, the presence of Cu_2O and Mn_3O_4 together could be explained by simultaneous release of O_2 by reactions (r7) and (r8) for CLOU. In addition, a new

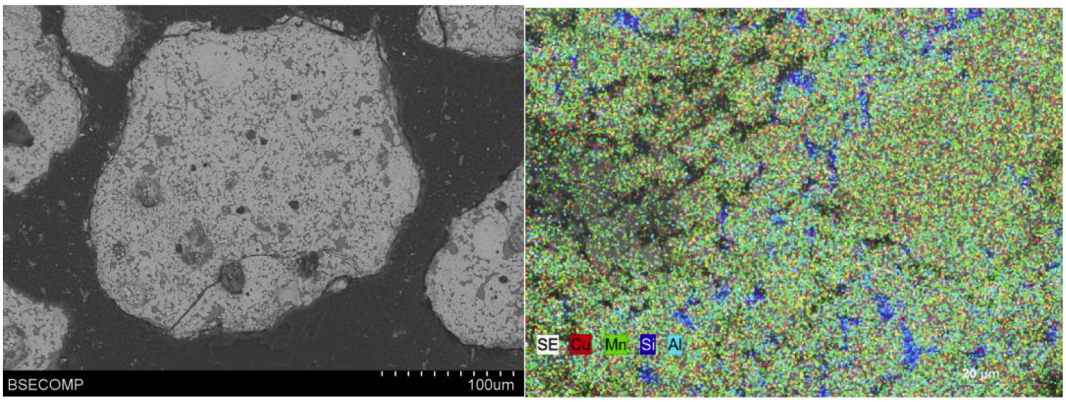

Fig. 4. (a) SEM scan of cross section; and (b) EDX mapping; of fresh CuMn80-Kao20 particles.

mixed oxide of Mn and Si (rodonite) appeared, $MnSiO_3$, which may come from interaction of Mn with Si in Kaolin. Rodonite comes from the reduction with CH_4, CO and H_2, of Mn_7SiO_{12} being its reactivity the lowest one with CH_4 [40] thus its contribution to the reduction would be negligible.

$$5Cu_{1.2}Mn_{1.8}O_4 \leftrightarrow 6CuMnO_2 + Mn_3O_4 + 2O_2 \quad \text{(r7)}$$

$$5Cu_{1.2}Mn_{1.8}O_4 \leftrightarrow 3Cu_2O + 3Mn_3O_4 + \frac{5}{2}O_2 \quad \text{(r8)}$$

While after reduction with CH_4, MnO and Cu appeared as main reduced species following (r9) for CLC. Then, (r10) shows the oxidation reaction.

$$5Cu_{1.2}Mn_{1.8}O_4 + 5CH_4 \rightarrow 6Cu + 9MnO + 5CO_2 + 10H_2O \quad \text{(r9)}$$

$$6Cu + 9MnO + \frac{11}{2}O_2 \rightarrow 5Cu_{1.2}Mn_{1.8}O_4 \quad \text{(r10)}$$

Table 1 shows the oxygen carrier chemical composition indicating that the main compounds active for CLC and CLOU were $Cu_{1.2}Mn_{1.8}O_4$ and Mn_3O_4. However, the presence of Mn_3O_4 reduced the oxygen transport capacity for CLOU because oxidation of Mn_3O_4 to Mn_2O_3 is very slow at 800 °C under the operating conditions, by thermodynamic limitations and hence, generally not giving O_2 by CLOU.

Oxygen transport capacity for CLC took a value of 12.5% that is slightly higher than the corresponding to the theoretical one for the reduction to MnO and Cu that is 11.1% taking into account the composition obtained by XRD and not pure compounds. It is possible that the remaining Mn_3O_4 and Mn_2O_3 in the particles increased the oxygen transport capacity of the oxygen carrier particles. For CLOU it was found a value of 4.1 wt%. The theoretical value for CLOU oxygen transport capacity taking into account the composition obtained by XRD and not pure compounds, varied between 4.0 wt% (r7) and 5.0 wt% (r8) as a function of the oxygen release dominant reaction. With the experimental value obtained in the TGA it could be proposed that the reaction r9 rules the oxygen release, with a small contribution of reaction r10. This fact was also corroborated with the low amount of Cu_2O found by XRD (3.8 wt%) after the reduction of the oxygen carrier in the TGA with N_2. Also, some of the original $Cu_{1.2}Mn_{1.8}O_4$ compound remained after reaction in N_2, suggesting that the reaction was not complete.

SEM analysis indicated that the inner of the particle was not completely smooth and had different crystalline structures, see Fig. 4. Some inclusions on the surface can be detected forming clusters. It can be observed two different surfaces; one rich in Cu—Mn mixed oxide formed by crystals of different size and a dark surface kaolin rich.

The EDX mapping confirmed some areas of differences in general, Cu—Mn in light crystals and Al and Si in dark networks. EDX analysis

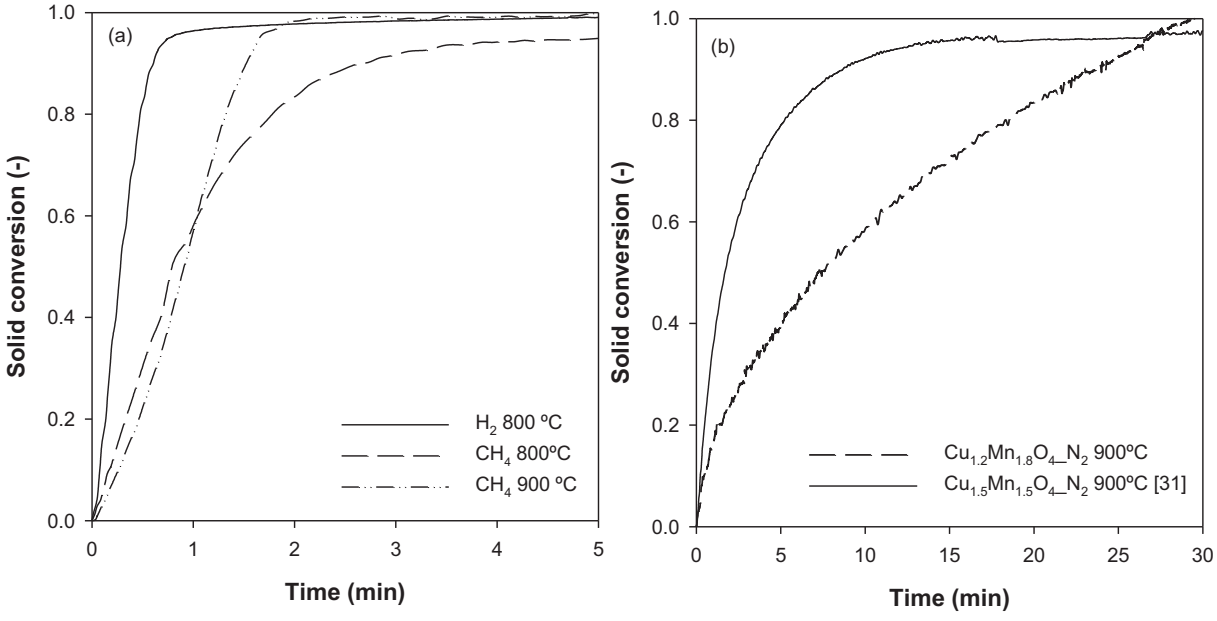

Fig. 5. Reduction conversion curves with: (a) H_2, CH_4; and (b) N_2 for the CuMn80-Kao20 and $Cu_{1.5}Mn_{1.5}O_4$ oxygen carrier from Adánez-Rubio et al. [31] at 950 °C.

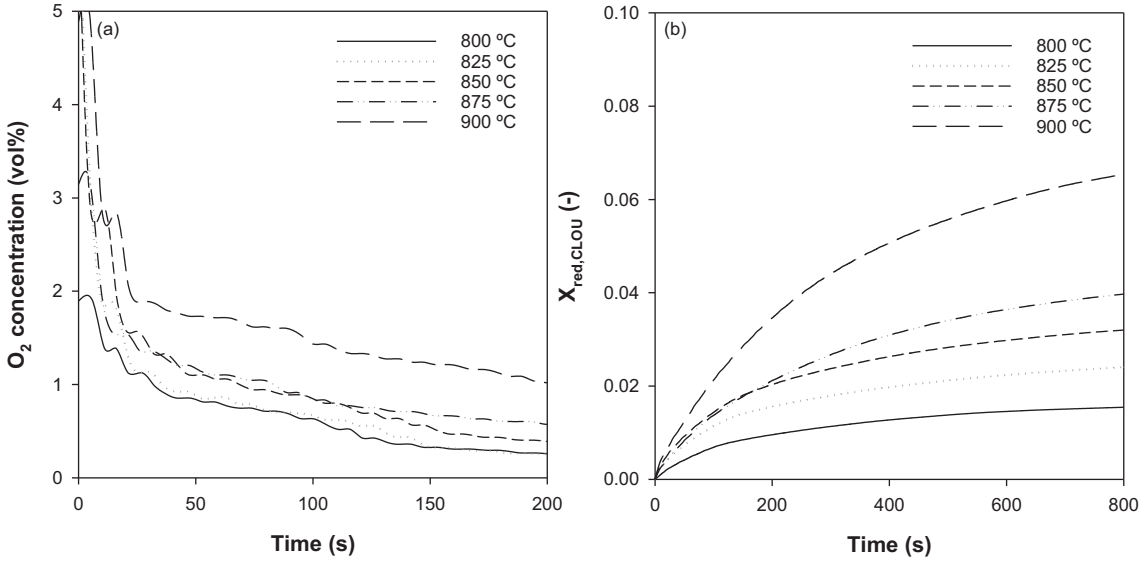

Fig. 6. (a) Oxygen concentration and (b) solid conversion profiles during the 3rd reduction cycle in N_2 at temperature from 800 to 900 °C.

performed on big area showed a good distribution throughout the particles of Cu—Mn mixed oxide and kaolin, both in the surface and in the inner of the particles.

3.2. Reactivity of oxygen carrier

Reactivity of the oxygen carrier was investigated in multiple redox cycles in N_2/air and CH_4 or H_2/air atmospheres at temperatures ranging from 800 to 950 °C in N_2 and at 800 to 900 °C in CH_4. Reactivity measured during reduction with CH_4 or H_2 gave one indication of the capacity of the oxygen carrier to supply lattice oxygen. Fig. 5a shows the evolution of the oxygen carrier conversion with CH_4, H_2 and N_2 at two different temperatures. Reduction with H_2 was very fast with a time for complete conversion lower than 1 min at 800 °C. With CH_4, complete conversion was reached in less than 2 min at 900 °C. For CLOU process, decomposition in N_2 was complete at reaction times lower than 30 min. A comparison with the CLOU reactivity found with $Cu_{1.5}Mn_{1.5}O_4$ oxygen carrier prepared with the same metal oxide composition although without kaolin is shown in Fig. 5b. The effect of kaolin can be clearly appreciated. Moreover, the change in the active compound from $Cu_{1.5}Mn_{1.5}O_4$ to $Cu_{1.2}Mn_{1.8}O_4$ could cause the important decrease in the reactivity increasing the complete conversion time from 10 to 30 min. Thus the effect of 20% kaolin reduced significantly the CLOU reactivity and the type of mixed oxide generated.

3.3. Batch fluidized bed reactor tests

In the batch fluidized bed reactor several redox cycles were carried out, in order to analyze the behavior of the oxygen carrier for O_2 release, the oxygen concentration used during oxidation step and the CH_4 combustion in a fluidized bed. To investigate the oxygen release in CLOU mode, three redox cycle experiments of 30 min were made in N_2/air atmospheres at temperatures from 800 to 900 °C.

The effect of the reaction temperature on the O_2 concentration released at pseudo equilibrium was investigated. Fig. 6 shows the oxygen concentration and the solid conversion profiles during the third cycle of reduction in N_2 in the temperature interval 800–900 °C with a step size of 25 °C.

Temperatures lower 900 °C in the fuel reactor would not significantly affect the purity of the CO_2–steam outlet mixture by presence of O_2 compared to the same temperature interval with free-copper oxide and manganese oxide, which showed higher O_2 partial pressure at

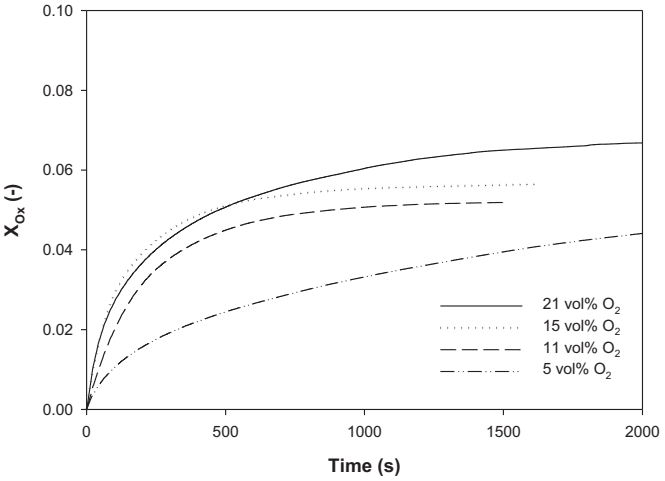

Fig. 7. Effect of the oxygen concentration in the oxygen carrier conversion during the oxidation at 850 °C at the batch fluidized bed reactor.

equilibrium conditions. Solid conversion (Fig. 6b) increased with the temperature although small conversions were found in the temperature window plotted.

The thermodynamics of the oxygen release by the oxygen carrier was used to determine the operating conditions for the air and fuel reactor in the continuous unit. To maximize the use of oxygen from air, the air reactor should work at temperatures below 850 °C. At these conditions the oxygen concentration in the air reactor exit would reach a maximum of 1.37 vol%. To analyze the effect of the oxygen concentration on the oxidation reaction, different experiments were made with four different oxygen concentrations ranging from 5 to 21% in the reactor. Fig. 7 shows the evolution of the solid conversion during the oxidation reaction at 850 °C. Previous reduction was made in 100% N_2 until during 30 min.

As shown in Fig. 7, there was a clear trend of decreasing the oxidation reaction rate with oxygen concentration decrease. This fact can be explained by the increase in the driving force for the oxidation by the difference between concentration at pseudo-equilibrium (1.37 vol% at 850 °C) and the inlet oxygen concentration. In the case of the oxidation carried out with 5 vol% O_2 it was necessary more than 30 min to reach

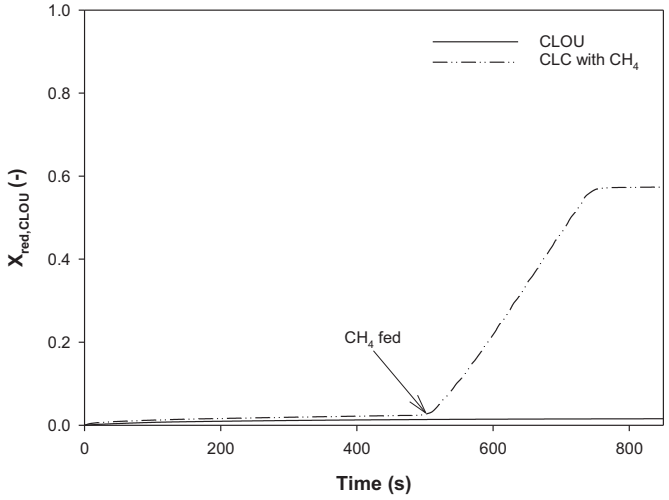

Fig. 8. Solid conversion based on CLOU oxygen transport capacity profiles during the 3rd reduction cycle with N_2 (CLOU) and with CH_4 (CLC) at 800 °C in the batch fluidized bed reactor.

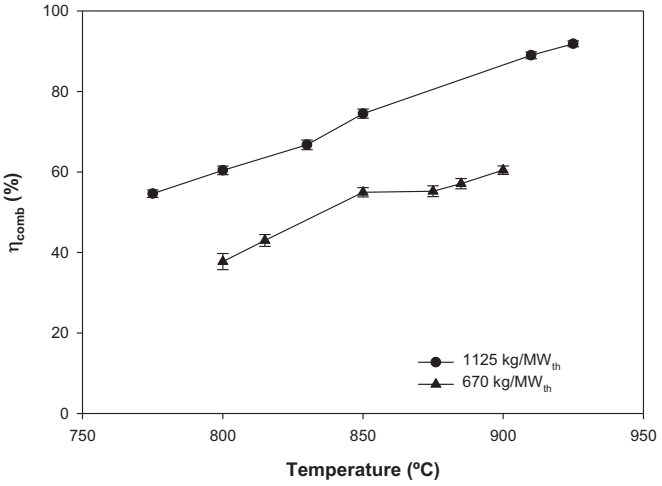

Fig. 9. Effect of the fuel reactor temperature on the combustion efficiency for to two oxygen carrier inventories used. T_{AR} = 810 °C. ϕ = 3–4. CH_4 = 15 vol%. N_2 to balance.

the same oxidation than in the previous cycles. For similar oxidation profiles it has been shown by TGA that the higher the oxygen concentration, the higher the oxidation reaction rate.

Once it was determined that the O_2 release by CLOU reaction took place without any agglomeration problem, the CH_4 combustion by the oxygen carrier was investigated at temperatures from 800 to 900 °C.

The experiments were carried out with 25 vol% CH_4, 20 vol% steam and 55 vol% N_2 at 750 and 800 °C. Fig. 8 shows a comparison of the oxygen carrier conversion with N_2 (CLOU) and with CH_4 (CLC). The solid conversion observed was much higher when the combustion mechanism was controlled by lattice oxygen (CLC) instead of CLOU, being 36 times higher for the same operation time.

These differences agree upon the results found by TGA indicating that the reactivity of this oxygen carrier to supply oxygen by CLOU mechanism was much lower than for CH_4 combustion. However, it was necessary to consider the driving force. The presence of CH_4 make that the driving force for the CLC mechanism was much higher than for the CLOU mechanism, obtaining a faster reaction of combustion against of oxygen release. Therefore, the oxygen carrier was tested in the 500 W_{th} unit using methane as main fuel.

3.4. Combustion in the 500 W_{th} CLC continuous unit

The oxygen carrier was evaluated for combustion of CH_4 and synthetic biogas (CO_2 + CH_4) in one 500 W_{th} CLC unit [41]. The effect of some operating variables on the combustion efficiency was evaluated. During all the experiments CO_2 never appeared at the air reactor outlet, indicating that there was not carbon bypass to this reactor and thus CO_2 capture was always 100%.

Experiments were performed to know the feasibility of using this oxygen carrier for CH_4 combustion, operating at high solid circulation rates; under these conditions low oxygen carrier conversion was obtained, because materials with high CuO concentration were known to suffer from agglomeration when they are reduced to Cu. Initial experiment with 7 vol% CH_4 using an oxygen carrier to fuel ratio of 28 operating at temperatures from 750 to 800 °C was carried out (tests C01 to C03 CH_4 in Table 2). After good fluidization without agglomeration, experiments continued to examine CH_4 concentration impact on the combustion efficiency using three different CH_4 concentrations (7, 11 and 15 vol%,) changing the solid circulation flowrate to maintain a near constant ϕ value of 15 (tests C04 to C06 CH_4 in Table 2). Combustion efficiency showed low values and increased with CH_4 concentration from 31.7 to 36.9 vol% using one oxygen carrier inventory of 670 kg/MW_{th}. This increase was considered due to the increase in the medium gas concentration in the reactor that increases reaction rates and also the combustion efficiency as concluded by [42].

The effect of the fuel reactor temperature on the combustion efficiency was investigated at temperatures from 775 to 925 °C using ϕ values between 9 and 11.7 (tests C07 to C20 CH_4 in Table 2). Moreover, this effect was investigated for two different oxygen carrier inventories of 670 and 1125 kg/MW_{th}, approximately. These different oxygen carrier inventories were obtained modifying the bed height using two different preheater/distributor plates for the fuel reactor. Fig. 9 shows the evolution of the combustion efficiency with temperature for both bed inventories. Efficiency increased significantly with the fuel reactor temperature, being more important for the higher inventory of oxygen carrier. Moreover, the important effect of the increase of the oxygen carrier inventory can be observed. Thus, to obtain high CH_4 combustion efficiencies with the CuMn80-Kao20 it was necessary to use high oxygen carrier inventories (higher than 1200 kg/MW) and fuel reactor temperatures as higher as 925 °C.

The regeneration is dependent of the air excess used in the air reactor for Cu—Mn oxygen carriers [30]. This fact was attributed to the increase in the CLOU contribution to the overall fuel conversion reaction. By this reason, the effect of the carrier oxidation in the air reactor on the combustion efficiency in the fuel reactor was also investigated (tests C07 to C10 CH_4 in Table 2). The effect of the air excess on the combustion efficiency was investigated using air excesses from 25 to 100% (thus [$O_{2,AR}$] varied from 17.86 to 21 vol%) at 800 °C. In this range of air excess the combustion efficiencies were similar, indicating that the oxidation is fast enough with common oxygen excess. Thus, the CH_4 combustion was mainly carried out by CLC reactions using lattice oxygen. The combustion efficiency should decrease when the air excess decreases under CLOU mechanism due to the high dependence of the oxygen concentration in the mixed oxides regeneration [30].

To confirm this assumption, experiments in the TGA with different H_2 and CH_4 concentrations were carried out in order to evaluate the concentrations in which combustion follow CLC or CLOU mechanisms. Fig. 10(a) depicts the effect of the H_2 concentration in the mass variation, ω, as a function of time for the reduction with different concentrations of H_2, from 1 to 15 vol% at 800 °C and for N_2 at 900 °C. In this case, the reaction mechanism was by lattice oxygen CLC. In order to compare with the CLOU reactivity obtained with pure N_2, Fig. 10(b) shows a logarithmic plot for the reaction rate as a function of the H_2 concentration. It is noteworthy that a linear relation existed between ln ($-r_{red,CLC}$) and ln[H_2] when the concentration of H_2 varied between

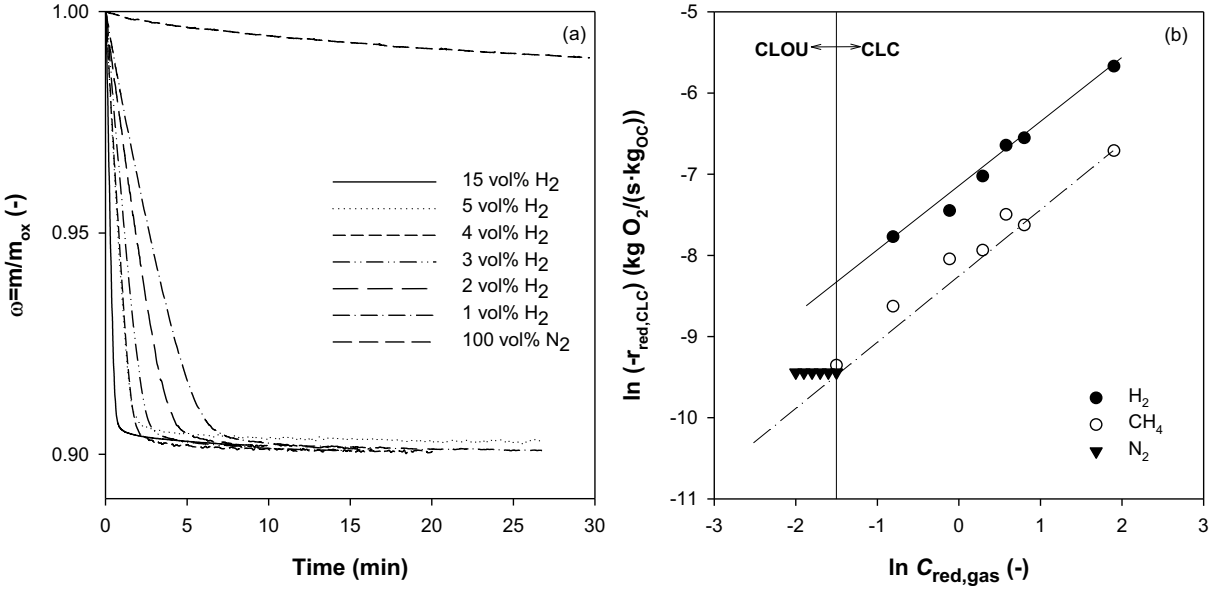

Fig. 10. (a) Effects of H_2 concentration on the reduction of the $Cu_{1.2}Mn_{1.8}O_4$ oxygen carrier; temperature: 800 (H_2) and 950 °C (N_2). (b) Reduction rates of $Cu_{1.2}Mn_{1.8}O_4$ as a function of the H_2 and CH_4 concentration.

values corresponding to 15 and 1 vol%. The reaction rates were higher than that found with N_2 at any H_2 concentration. This behavior was different to that found by Mei et al. with $Cu/CuAl_2O_4$ [43] and also studied by Su et al. [44] in which the CLC mechanism was faster than the CLOU mechanism at H_2 concentrations higher than 1 vol%.

The same analysis was done using CH_4 as fuel, because it was the fuel used in the continuous unit. Thus, it was possible to observe that also the reaction rate decrease when the CH_4 concentration decrease. However, when the CH_4 concentration decreased below 0.5 vol%, i.e. ln [CH_4] = −1.5, a reduction rate of 0.08 × 10^{-3} $kgO_2/(s{\cdot}kgOC)$ was observed, which is equal to the oxygen release rate by CLOU, as it can be seen in Fig. 10(b). As a consequence, the oxygen uncoupling reaction was faster than the gas–solid reaction (lattice oxygen) at low CH_4 concentrations, and therefore the oxygen transference rate was dominated by oxygen uncoupling mechanism.

As a conclusion, when CH_4 was used as fuel at concentrations higher than 0.5 vol%, the combustion mechanism can be considered controlled by lattice oxygen transference via gas-solid reaction, and the reaction rate increases with the fuel concentration. On the contrary, oxygen uncoupling dominated the combustion of CH_4 at concentrations lower than 0.5 vol%, which means that the oxygen transference rate was dominated by the rate of oxygen release, whereas CH_4 concentration contributed little to the reduction of $Cu_{1.2}Mn_{1.8}O_4$ to $CuMnO_2$. Thus, in the upper part of a fuel reactor when low CH_4 concentrations were present, CLOU mechanism of oxygen supply would be responsible of reaching complete CH_4 combustion.

3.5. Synthetic biogas combustion

One option of interest is to use this oxygen carrier in Chemical Looping Combustion of biogas. Biogas is generated mainly by waste digestion and contains important amounts of CO_2. Typical biogas contains one CO_2/CH_4 ratio of 1.5 and variable amounts of sulphur compounds. To check the suitability of CLC with the developed oxygen carrier, one experimental campaign was developed in the continuous unit using synthetic biogas. Experiments were performed in the 500 W_{th} CLC unit burning synthetic biogas with different ratios CO_2/CH_4 from 0.7 to 3 at temperatures from 775 to 920 °C and oxygen carrier to fuel ratios from 4.5 to 12 (tests C01 to C17 BIO in Table 2). CO_2 never appeared at the air reactor outlet, indicating also in this case there was no carbon bypass to this reactor and thus CO_2 capture was 100%.

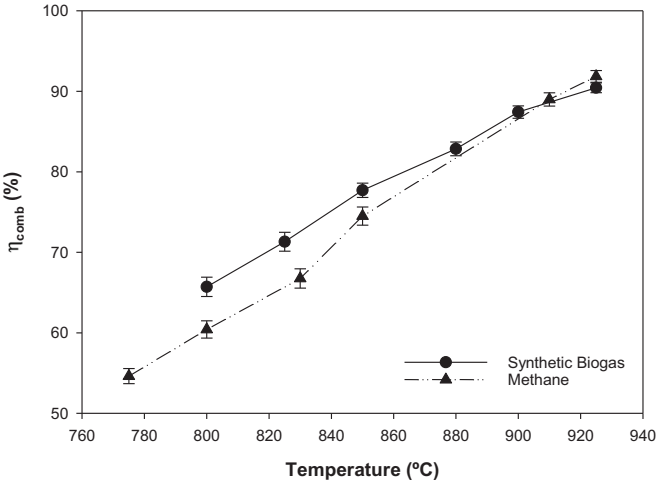

Fig. 11. Combustion efficiency profile for fuel reactor temperature burning synthetic biogas (full line) with CO_2/CH_4 ratio of 1.5 and ϕ around 3.1. Combustion efficiency profile for fuel reactor temperature burning 15% CH_4 (—···), ϕ = 3.1.

3.5.1. Effect of the CO_2/CH_4 concentration ratio

Biogas with five CO_2/CH_4 concentration ratios from 0.7 to 3 was used for the combustion in the 500W_{th} continuous unit at 800 °C using a ϕ value of 9.3. It can be seen that the ratio CO_2/CH_4 did not affect the combustion efficiency as can be observed in Table 2 (tests C01 to C05 Bio), with a value around 65% in all the interval of CO_2/CH_4 ratio studied.

3.5.2. Effect of the fuel reactor temperature

The effect of the fuel reactor temperature on the combustion efficiency is shown in Fig. 11. As expected, efficiency showed an important increase with temperature, although the same value of 20% CH_4 was used in the different CO_2/CH_4 mixtures. For comparison purposes, the line corresponding to 15% CH_4 combustion with the same solid

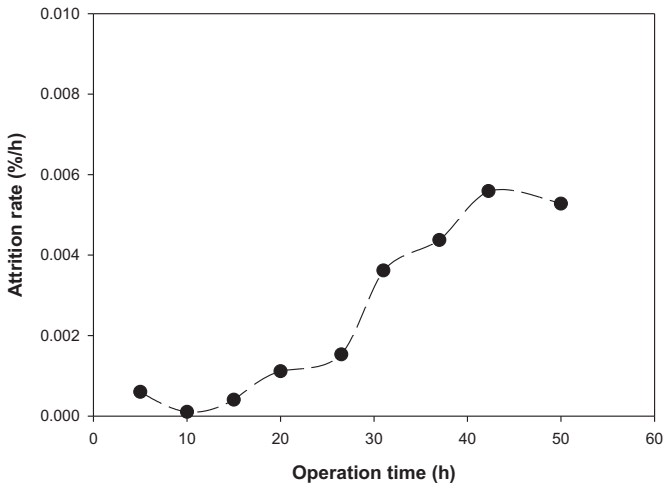

Fig. 12. Attrition rate in the continuous unit measured during 50 h of combustion in steps of about 5 h.

inventory (1125 kg/MW_{th}) has also been included. Some differences were observed especially at temperatures lower than 890 °C that can be attributed to the higher CH_4 concentration used. So, it can be said that the possible CH_4 dry reforming by the CO_2 with the biogas fed in the fuel reactor did not significantly affect the CLC combustion process using CuMn80-Kao20 as oxygen carrier.

3.5.3. Effect of the oxygen carrier to fuel ratio

The oxygen carrier circulation rate is directly correlated to the oxygen carrier/fuel ratio (ϕ) which should impact on the reaction rates. Experiments with oxygen carrier to fuel ratios from 4.5 to 12 at 850 °C and CO_2/CH_4 ratio of 1.5 were done to analyze the effect of this variable on the combustion efficiency. Low ϕ ratios, from 1 to 3, are usually sufficient to reach complete combustion with Cu based oxygen carriers. In the present study low ratios were not used to avoid the risk of agglomeration when an oxygen carrier with more than 20% CuO [18] is used as in this case. Combustion efficiencies as a function of ϕ are indicated in Table 2 (tests C06 and C15 to C17 Bio). Low combustion efficiencies were found for all the ϕ values, showing the low reactivity of this material with respect to other Cu based oxygen carriers when oxygen carrier inventories of 930 kg/MW_{th} were used. A non-significant tendency between the combustion efficiency and ϕ was observed with values around 75%. This behavior corresponds to the last part, with very low slope, in the combustion efficiency versus ϕ plots found for all the oxygen carriers, although for this temperature and one oxygen carrier inventory of 930 kg/MW_{th} was placed at low combustion efficiencies (75%) [45]. Thus, to reach complete combustion of CH_4 or synthetic biogas the use of higher inventories with the high ϕ values used was necessary.

The effect of the air excess was also tested during biogas combustion at air excess ranging from 20 to 50% at 850 °C. Also in this case, the effect on the combustion efficiency was not significantly affected, confirming the results found for the CH_4 combustion. Thus, the oxygen supply for the combustion can be considered coming from lattice oxygen. It can be concluded that the biogas combustion was carried out by lattice oxygen supply mechanism, as when CH_4 was used as fuel. Taking into account the above results, for this low reactivity oxygen carrier, the main operating variables were found the fuel reactor temperature and the oxygen carrier inventory, when the process was carried out at high ϕ values in order to avoid agglomeration in the bed.

3.6. Attrition behavior

Oxygen carriers undergo attrition during fluidized bed CLC reaction; this fact determines the lifetime of the material and the needs of replacement of the material lost during reaction. Attrition was measured during 26 h of redox cycles in the batch reactor. Values measured during CLOU operation with redox cycles N_2/air were 5.10^{-5} wt%/h while combustion cycles burning CH_4 showed higher values of 1.3. 10^{-3} wt %/h. These values indicated a good mechanical stability of the oxygen carrier. The mixed oxide $Cu_{1.5}Mn_{1.5}O_4$ developed by Adanez-Rubio et al. [31] prepared without kaolin showed an attrition rate of 5. 10^{-3} wt%/h after 35 h cycles in N_2/air. A comparison between these two oxygen carriers indicated a 100 times lower attrition rate for the oxygen carrier prepared with the addition of kaolin.

In the continuous unit, the attrition rate was calculated from the fines of size lower than 45 μm recovered after each 5 h of operation. This evaluation was considered as the nearest to the real behavior of the oxygen carrier in an industrial unit. Fig. 12 plots the attrition rate as a function of the operation time. In the first 10 h of continuous operation, it can be observed a decrease in the attrition rate. This is attributed to rounding effects of the particles and to the loses of possible fines stuck to the particles. After this minimum, the increase of the attrition rate is related with new fines formed during the redox cycles. The first 26.5 h results were obtained during CH_4 combustion, while points from 26.5 h to 50 h corresponded to synthetic biogas combustion. The initial values increased with the combustion time reaching a value of 5.3 10^{-3} wt%/h. From this attrition rate a lifetime of the oxygen was extrapolated to be 19,000 h.

It can be said that this oxygen carrier exhibited the highest lifetime found for a Cu based oxygen carrier. Up to now the highest value for a Cu oxygen carrier impregnated on γ-Al_2O_3 was 5000 h [22]. This fact clearly showed the strong effect of the presence of 20% kaolin on its composition on the lifetime although at the same time, there was an important decrease in the reactivity and performance for CLC combustion. Thus, in order to optimize this oxygen carrier, it is necessary to meet a compromise between lifetime and reactivity and likely lower fractions of kaolin would be used on its composition. Table 3 shows the attrition rate and extrapolated lifetime for several CLC oxygen carriers using methane as fuel in a continuous unit found in the literature. It can

Table 3
Relevant information on the use of oxygen-carrier in CLC units for natural gas.

Oxygen carrier	Unit size (kW_{th})	Operation time (h)	Temp. (°C)		Attrition rate (%/h)	Lifetime (h)	Ref.
			FR	AR			
NiO/Al_2O_3	10	100	≈900	1000	0.0023	40,000	[46]
$NiO/NiAl_2O_4$+ $MgAl_2O_4$	10	1016	≈940	1000	0.003	33,000	[47]
$NiO/NiAl_2O_4$	10	160	≈940	1000	0.022	4500	[48]
NiO/α-Al_2O_3	0.5	70	880	950	0.01	10,000	[49]
CuO/γ-Al_2O_3	10	100	800	800	0.04	2400	[12]
CuO/γ-Al_2O_3	0.5	60	800	900	0.09	1100	[50]
CuO14/γAl_2O_3 Commercial	0.5	60	800	850	0.02	5000	[22]
$Ca_{0.9}Mg_{0.1}Mn_{0.9}O_{3-\delta}$	0.5	54	900	900	0.09	1100	[51]
Fe_2O_3/Al_2O_3	0.5	46	950	950	0.09	1100	[52]
CuMn80-Kao20	0.5	50	800–900	800–850	0.0053	19,000	Present work

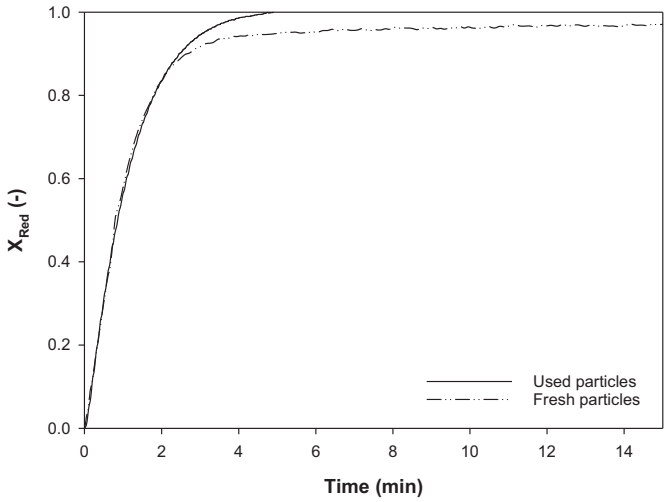

Fig. 13. Results from TGA at CH_4 800 °C for fresh and used oxygen carrier.

be observed that the CuMn80-Kao20 has the lowest attrition rate of the Cu-based oxygen carriers for methane combustion, and is in the same order than the Ni-based oxygen carriers.

3.7. Oxygen carrier characterization after use

The chemical and physical properties of the oxygen carrier after 95 h of hot fluidization with around 50 h of combustion were analyzed. Main results are shown in Table 1. The oxygen transport capacity increased from 12.5 to 13.1% and the porosity increased up to 44% as a consequence of the 50 h of the CLC combustion. The crushing strength of particles slightly decreased to 2.1 N, while the attrition jet index (AJI) showed one increase from 0.9 to 11.2 indicating the reduction of the particle mechanical integrity although the attrition rates found were very low (5.3 10^{-3} wt%/h).

Oxygen carrier reactivity with CH_4 was maintained stable after 50 h of operation in the 500 W_{th} continuous unit burning CH_4 and synthetic biogas as it can be observed in Fig. 13.

In order to answer the final question of the oxygen carrier composition over time, XRD patterns on particles after 50 h combustion from both reactors were obtained. The phases that could be identified were $Cu_{1.2}Mn_{1.8}O_4$, $CuMnO_2$, Mn_3O_4, Cu_2O and Cu. In the air reactor sample, the same compounds were found with different intensities with the exception of Cu.

A sample of used particles taken from the fuel reactor after 50 h of combustion was characterized by SEM-EDX. Particles showed a superficial and internal porosity, see Fig. 14. The inspection of the surface (Fig. 14 a and b) suggested a good distribution of Cu—Mn mixed oxides without any darker area rich in kaolin. With EDX mapping a low amount of copper is detected on the surface. From the cross section analysis in Fig. 14 c and d, larger differences of element distribution were observed, with more silicon and aluminum towards the edges of the particles and copper in larger extent in the core of the particles (lighter areas).

4. Conclusions

The effect of the addition of kaolin as ceramic binder on the characteristics as oxygen carrier of a Cu—Mn mixed oxide were examined from the chemical, mechanical and redox points of view.

Addition of 20% kaolin changed the chemical composition of the mixed oxide obtaining $Cu_{1.2}Mn_{1.8}O_4$ and significantly improving the mechanical resistance of the oxygen carrier.

Reactivity of the oxygen carrier for oxygen release by CLOU process underwent an important decrease with respect to the similar oxygen carrier prepared without kaolin.

The material was first evaluated in a batch fluidized bed reactor. The pseudo equilibrium O_2 release was reached between the solid phases

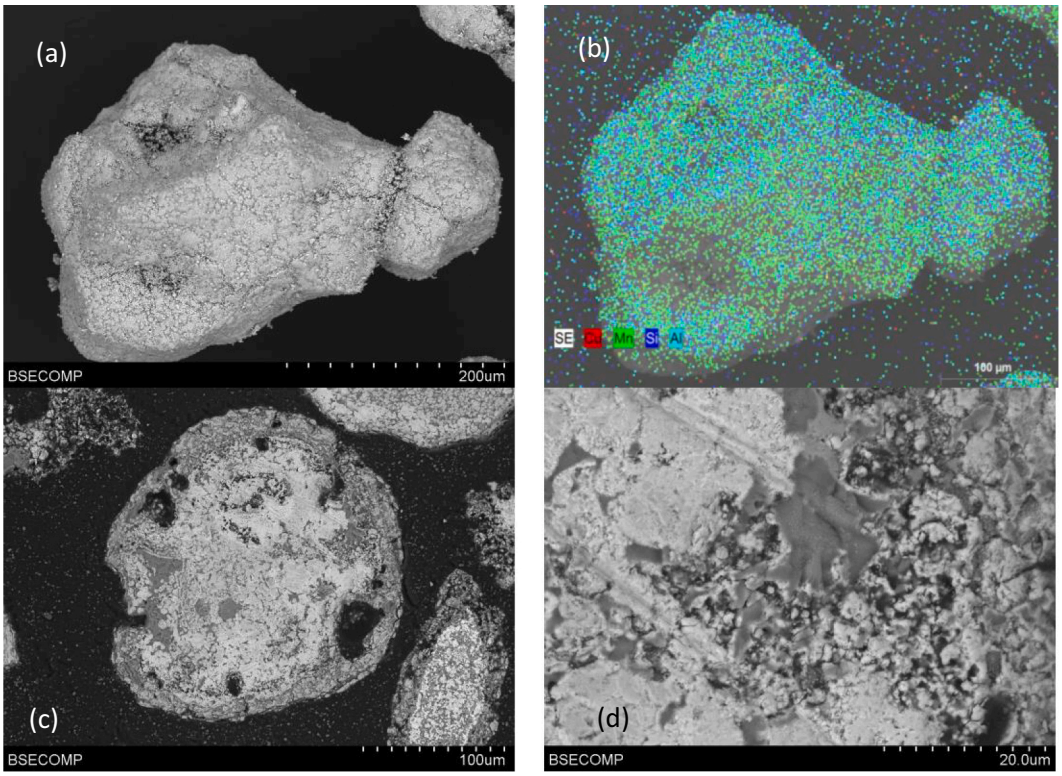

Fig. 14. SEM images of CuMn80-Kao20 collected from the fuel reactor after 50 h of continuous combustion (a) Surface of used particle(b). EDX mapping of the surface for Cu Mn Si and Al (c, d). Cross of used particle.

between $Cu_{1.2}Mn_{1.8}O_4$ and CuO, with 1.1 vol% at 800 °C and 2.2 vol% at 900 °C. Although O_2 concentration was enough for solid fuel combustion by CLOU process its reactivity was low for its use in this type of process.

The oxygen carrier was used for CH_4 combustion in a CLC continuous unit for 50 h at temperatures up to 925 °C and no agglomeration problems were observed during the continuous operation at oxygen carrier to fuel ratios higher than 3.

To reach complete methane or synthetic biogas combustion to CO_2 and H_2O oxygen carrier inventories higher than 1200 kg/MW_{th} and fuel reactor temperatures of 925 °C were needed. Results found during biogas combustion were similar to that found during methane combustion.

During gaseous fuel combustion, the mechanism of oxygen supply was by lattice oxygen in the main part of reactor height, being CLOU mechanism only significant if CH_4 concentrations were lower than 0.5%.

Presence of kaolin increases the extrapolated lifetime of the oxygen carrier to a value of 19,000 h that is over 3.6 times to the value for a Cu based oxygen carrier in CLC.

Addition of kaolin had one important effect on the attrition resistance of the oxygen carrier although the reactivity decreases both for CLOU and CLC reactions. Thus, it is necessary to optimize the kaolin content in order to obtain a tradeoff between attrition resistance and oxygen carrier reactivity.

Declaration of Competing Interest

The authors declare that they have no known competing financial interests or personal relationships that could have appeared to influence the work reported in this paper.

Acknowledgment

The work presented in this article is partially funded by the Spanish Research Council (CSIC) through the Intramural Project (201980E043), and by the European Regional Development Fund (ERDF) under the program “Programa Operativo FEDER Aragón 2014-2020 - Construyendo Europa desde Aragón. Project BiosinCO2 (LMP180_18).

References

[1] IEA, Global Energy & CO_2 Status Report 2019, IEA, Paris (France), 2019.
[2] ONU, United Nations Framework Convention for Climate Change, The Paris Agreement, ONU, Paris (France), 2015.
[3] M.M. Hossain, H.I. de Lasa, Chemical-looping combustion (CLC) for inherent CO_2 separations—a review, Chem. Eng. Sci. 63 (2008) 4433–4451.
[4] A. Lyngfelt, A. Brink, Ø. Langørgen, T. Mattisson, M. Rydén, C. Linderholm, 11,000 h of chemical-looping combustion operation—where are we and where do we want to go? Int. J. Greenh Gas Control 88 (2019) 38–56.
[5] A. Lyngfelt, Chemical looping combustion: status and development challenges, Energy Fuel 34 (2020) 9077–9093.
[6] L.S. Fan, Chemical Looping Systems for Fossil Energy Conversions, 2010.
[7] H. Zhao, X. Tian, J. Ma, M. Su, B. Wang, D. Mei, Development of tailor-made oxygen carriers and reactors for chemical looping processes at Huazhong University of Science & Technology, Int. J. Greenh Gas Control 93 (2020).
[8] J. Adanez, A. Abad, F. Garcia-Labiano, P. Gayan, L. de Diego, Progress in chemical-looping combustion and reforming technologies, Prog. Energy Combust. Sci. 38 (2012) 215–282.
[9] J. Adánez, A. Abad, T. Mendiara, P. Gayán, L.F. de Diego, F. García-Labiano, Chemical looping combustion of solid fuels, Prog. Energy Combust. Sci. 65 (2018) 6–66.
[10] A. Zylka, J. Krzywanski, T. Czakiert, K. Idziak, M. Sosnowski, K. Grabowska, T. Prauzner, W. Nowak, The 4th Generation of CeSFaMB in numerical simulations for CuO-based oxygen carrier in CLC system, Fuel 255 (2019).
[11] A. Zylka, J. Krzywanski, T. Czakiert, K. Idziak, M. Sosnowski, M.L. de Souza-Santos, K. Sztekler, W. Nowak, Modeling of the chemical looping combustion of hard coal and biomass using ilmenite as the oxygen carrier, Energies 13 (2020).
[12] L.F. de Diego, F. García-Labiano, P. Gayán, J. Celaya, J.M. Palacios, J. Adánez, Operation of a 10kW_{th} chemical-looping combustor during 200h with a CuO–Al_2O_3 oxygen carrier, Fuel 86 (2007) 1036–1045.
[13] T. Mattisson, A. Lyngfelt, H. Leion, Chemical-looping with oxygen uncoupling for combustion of solid fuels, Int. J. Greenh Gas Control 3 (2009) 11–19.
[14] P. Gayán, I. Adánez-Rubio, A. Abad, L.F. de Diego, F. García Labiano, J. Adánez, Development of Cu-based oxygen carriers for Chemical-Looping with Oxygen Uncoupling (CLOU) process, Fuel 96 (2012) 226–238.
[15] M. Rydén, H. Leion, T. Mattisson, A. Lyngfelt, Combined oxides as oxygen-carrier material for chemical-looping with oxygen uncoupling, Appl. Energy 113 (2014) 1924–1932.
[16] A. Abad, I. Adánez-Rubio, P. Gayán, F. García-Labiano, L. de Diego, J. Adánez, Demonstration of chemical-looping with oxygen uncoupling (CLOU) process in a 1.5 kW_{th} continuously operating unit using a Cu-based oxygen-carrier, Int. J. Greenh Gas Control 6 (2012) 189–200.
[17] K.M. Merrett, K.J. Whitty, Evaluation of coal conversion pathways in fluidized bed chemical looping combustion with oxygen uncoupling (CLOU), Fuel 258 (2019).
[18] L.F. de Diego, F. Garcia-Labiano, J. Adánez, P. Gayán, A. Abad, B.M. Corbella, J. Maria Palacios, Development of Cu-based oxygen carriers for chemical-looping combustion, Fuel 83 (2004) (1749-1757).
[19] J. Adánez, P. Gayán, J. Celaya, L.F. de Diego, F. García-Labiano, A. Abad, Chemical looping combustion in a 10 kW_{th} prototype using a CuO/Al_2O_3 oxygen carrier: effect of operating conditions on methane combustion, Ind. Eng. Chem. Res. 45 (2006) 6075–6080.
[20] O. Langørgen, I. Saanum, N.E.L. Haugen, Chemical looping combustion of methane using a copper-based oxygen carrier in a 150 kW reactor system, Energy Procedia 114 (2017) 352–360.
[21] R.F. Pachler, S. Penthor, K. Mayer, H. Hofbauer, Investigation of the fate of nitrogen in chemical looping combustion of gaseous fuels using two different oxygen carriers, Energy 195 (2020).
[22] A. Cabello, P. Gayán, A. Abad, L.F. de Diego, F. García-Labiano, M.T. Izquierdo, A. Scullard, G. Williams, J. Adánez, Long-lasting Cu-based oxygen carrier material for industrial scale in chemical looping combustion, Int. J. Greenh Gas Control 52 (2016) 120–129.
[23] I. Adánez-Rubio, A. Abad, P. Gayán, L.F. de Diego, F. García-Labiano, J. Adánez, Biomass combustion with CO_2 capture by chemical looping with oxygen uncoupling (CLOU), Fuel Process. Technol. 124 (2014) 104–114.
[24] I. Adánez-Rubio, A. Pérez-Astray, T. Mendiara, M.T. Izquierdo, A. Abad, P. Gayán, L.F. de Diego, F. García-Labiano, J. Adánez, Chemical looping combustion of biomass: CLOU experiments with a Cu-Mn mixed oxide, Fuel Process. Technol. 172 (2018) 179–186.
[25] I. Adánez-Rubio, A. Pérez-Astray, A. Abad, P. Gayán, L.F. De Diego, J. Adánez, Chemical looping with oxygen uncoupling: an advanced biomass combustion technology to avoid CO_2 emissions, Mitig. Adapt. Strateg. Glob. Chang. 24 (2019).
[26] F.C.M. Driessens, G.D. Rieck, Phase equilibria in the system Cu-Mn-O, Zeitschrift fuer Anorganische und Allgemeine Chemie 351 (1967).
[27] A.-M. Azad, A. Hedayati, M. Rydén, H. Leion, T. Mattisson, Examining the Cu–Mn–O spinel system as an oxygen carrier in chemical looping combustion, Energ. Technol. 1 (2013) 59–69.
[28] D. Hosseini, Q. Imtiaz, P.M. Abdala, S. Yoon, A.M. Kierzkowska, A. Weidenkaff, C. R. Müller, CuO promoted Mn_2O_3-based materials for solid fuel combustion with inherent CO_2 capture, J. Mater. Chem. A 3 (2015) 10545–10550.
[29] I. Adánez-Rubio, A. Abad, P. Gayán, I. Adánez, L.F. De Diego, F. García-Labiano, J. Adánez, Use of hopcalite-derived Cu-Mn mixed oxide as oxygen carrier for chemical looping with oxygen uncoupling process, Energy Fuel 30 (2016) 5953–5963.
[30] I. Adánez-Rubio, P. Gayan, A. Abad, L.F. de Diego, F. García-Labiano, J. Adánez, Coal combustion by a spray granulated Cu-Mn mixed oxide for CLOU process, Appl. Energy 208 (2017) 561–570.
[31] I. Adánez-Rubio, M.T. Izquierdo, A. Abad, P. Gayan, L.F. de Diego, J. Adánez, Spray granulated Cu-Mn oxygen carrier for chemical looping with oxygen uncoupling (CLOU) process, Int. J. Greenh Gas Control 65 (2017) 76–85.
[32] I. Adánez-Rubio, A. Abad, P. Gayan, L.F. de Diego, J. Adánez, CLOU process performance with a Cu-Mn oxygen carrier in the combustion of different types of coal with CO_2 capture, Fuel 212 (2018) 605–612.
[33] A. Pérez-Astray, I. Adánez-Rubio, T. Mendiara, M.T. Izquierdo, A. Abad, P. Gayán, L.F. de Diego, F. García-Labiano, J. Adánez, Comparative study of fuel-N and tar evolution in chemical looping combustion of biomass under both *i*G-CLC and CLOU modes, Fuel 236 (2019) 598–607.
[34] ASTM, Standard Test Method for Determination of Attrition of FCC Catalyst by Air Jets. ASTM D5757–11., Standard Test Method for Determination of Attrition of FCC Catalyst by Air Jets, 2006.
[35] J. Adánez, L.F. de Diego, F. García-Labiano, P. Gayán, A. Abad, J.M. Palacios, Selection of oxygen carriers for chemical-looping combustion, Energy Fuel 18 (2004) 371–377.
[36] I. Adánez-Rubio, P. Gayán, A. Abad, L.F. de Diego, F. García-Labiano, J. Adánez, Evaluation of a spray-dried CuO/$MgAl_2O_4$Oxygen carrier for the chemical looping with oxygen uncoupling process, Energy Fuel 26 (2012) 3069–3081.
[37] C.R. Forero, P. Gayán, L.F. de Diego, A. Abad, F. García Labiano, J. Adánez, Syngas combustion in a 500 W_{th} chemical-looping combustion system using an impregnated Cu-based oxygen carrier, Fuel Process. Technol. 90 (2009) 1471–1479.
[38] M. Johansson, T. Mattisson, A. Lyngfelt, Investigation of Fe_2O_3 with $MgAl_2O_4$ for chemical-looping combustion, Ind. Eng. Chem. Res. 43 (2004) 6978–6987.
[39] L.T. Drzal, J.P. Rynd, T. Fort Jr., Effects of calcination on the surface properties of kaolinite, J. Colloid Interface Sci. 93 (1983) 126–139.
[40] F.J. Velasco-Sarria, C.R. Forero, I. Adánez-Rubio, A. Abad, J. Adánez, Assessment of low-cost oxygen carrier in South-western Colombia, and its use in the in-situ gasification chemical looping combustion technology, Fuel 218 (2018) 417–424.
[41] A. Nilsson, Performance of a new Cu-based oxygen carrier in a 500 W continuous Chemical Looping Combustion unit for gaseous fuels, in: Chemistry and Chemical Engineering, Division of Environmental Inorganic Chemistry Chalmers University of Technology, Gothenburg, Sweden, 2020.

[42] A. Abad, J. Adánez, F. García-Labiano, L. de Diego, P. Gayán, J. Celaya, Mapping of the range of operational conditions for Cu-, Fe-, and Ni-based oxygen carriers in chemical-looping combustion, Chem. Eng. Sci. 62 (2007) 533–549.
[43] D. Mei, A. Abad, H. Zhao, J. Adánez, Characterization of a sol-gel derived CuO/$CuAl_2O_4$ oxygen carrier for chemical looping combustion (CLC) of gaseous fuels: relevance of gas-solid and oxygen uncoupling reactions, Fuel Process. Technol. 133 (2015) 210–219.
[44] M. Su, H. Zhao, X. Tian, The competition between direct gas–solid reduction and oxygen uncoupling of CuO oxygen carrier in chemical looping with oxygen uncoupling: a single particle simulation study, Combust. Flame 221 (2020) 219–227.
[45] I. Adánez-Rubio, S.T. Bararpour, A. Abad, P. Gayán, G. Williams, A. Scullard, N. Mahinpey, J. Adánez, Performance Evaluation of a Cu-based oxygen carrier impregnated onto ZrO_2 for chemical-looping combustion (CLC), Ind. Eng. Chem. Res. 59 (2020) 7255–7266.
[46] A. Lyngfelt, H. Thunman, Construction and 100 h of operational experience of A 10-kW chemical-looping combustor, in: Carbon Dioxide Capture for Storage in Deep Geologic Formations, 2005, pp. 625–645.
[47] C. Linderholm, T. Mattisson, A. Lyngfelt, Long-term integrity testing of spray-dried particles in a 10-kW chemical-looping combustor using natural gas as fuel, Fuel 88 (2009) 2083–2096.
[48] C. Linderholm, A. Abad, T. Mattisson, A. Lyngfelt, 160 h of chemical-looping combustion in a 10 kW reactor system with a NiO-based oxygen carrier, Int. J. Greenh Gas Control 2 (2008) 520–530.
[49] J. Adánez, C. Dueso, L.F. de Diego, F. García-Labiano, P. Gayán, A. Abad, Methane combustion in a 500 W_{th} chemical-looping combustion system using an impregnated ni-based oxygen carrier, Energy Fuel 23 (2009) 130–142.
[50] C.R. Forero, P. Gayán, F. García-Labiano, L.F. de Diego, A. Abad, J. Adánez, High temperature behaviour of a CuO/γAl_2O_3 oxygen carrier for chemical-looping combustion, Int. J. Greenh Gas Control 5 (2011) 659–667.
[51] A. Cabello, A. Abad, P. Gayán, L.F. de Diego, F. García-Labiano, J. Adánez, Effect of operating conditions and H_2S presence on the performance of $CaMg_{0.1}Mn_{0.9}O_{3-\delta}$ perovskite material in chemical looping combustion (CLC), Energy Fuel 28 (2014) 1262–1274.
[52] P. Gayán, M.A. Pans, M. Ortiz, A. Abad, L.F. De Diego, F. García-Labiano, J. Adánez, Testing of a highly reactive impregnated Fe_2O_3/Al_2O_3 oxygen carrier for a SR-CLC system in a continuous CLC unit, Fuel Process. Technol. 96 (2012) 37–47.